Proceedings of IMECE 2008
2008 ASME International Mechanical Engineering Congress and Exposition
October 31-November 6, 2008, Boston, Massachusetts, USA

ASME2008-67861

CHARACTERIZATION AND MODELING OF CAPACITIVE MICROMACHINED ULTRASONIC TRANSDUCERS FOR DIAGNOSTIC ULTRASOUND

Christopher B. Doody and Robert D. White*
Mechanical Engineering Department, Tufts University
Medford, MA 02155, USA
r.white@tufts.edu

Jaspreet S. Wadhwa and David F. Lemmerhirt
Sonetics Ultrasound, Inc.
Ann Arbor, MI 48109, USA

ABSTRACT

This paper describes the characterization and modeling of capacitive micromachined ultrasonic transducers (cMUTs). Computational models of the transducers were produced through the combined use of finite element analysis (FEA) and lumped element modeling. Frequency response plots were generated for both transducers in air and water environments. Through the use of laser Doppler velocimetry, transient step response and frequency sweep tests were performed on single array elements. These measurements are compared to the predicted results represented in the models. The computational results for both coupled and uncoupled arrays are compared, and show a significant increase in the array bandwidth due to coupling. Frequency sweep tests were also performed on column array elements, and results were compared between driven and adjacent, non-driven columns.

INTRODUCTION

Diagnostic medical ultrasound requires arrays of ultrasound transducers for both transmit and receive operations. Piezoelectric crystals or piezocomposites have been utilized for most existing commercial technology. Recently, capacitive micromachined ultrasound transducers (cMUTs) have become a competing MEMS technology with some attractive features; particularly the possibility of integrating signal processing, signal routing, and power electronics on chip with the transducers, and also the possibility of increased bandwidth.

The design of cMUTs has been studied since the early 1990's [1]. Researchers have described a variety of cMUT designs and models [1-2]. Both lumped element modeling and finite element analysis (FEA) have been employed [3-4]. Measurements of device response often include transmit and receive frequency response measurements in a water tank, and also device input electrical impedance [1-2]. Laser interferometry has also been used in at least one case to characterize cMUT dynamics [5].

This paper presents a hybrid finite element/lumped element modeling scheme for cMUT arrays, and compares the predictions to laser Doppler velocimetry measurements. The cMUTs being tested were fabricated using layers common to standard commercial CMOS processes. For this project, two designs of micromachined ultrasonic array elements were considered.

MODELING

Lumped Element Modeling

Lumped element acoustic models were used in order to create a computational model of the transducers. Two coupled electrical-mechanical acoustic models of a single cMUT element can be seen in Figure 1. The top model represents the element in "transmit" mode. In "transmit" mode, the driving RF voltage, V_{ac}, is applied to the

*Address all correspondence to this author.

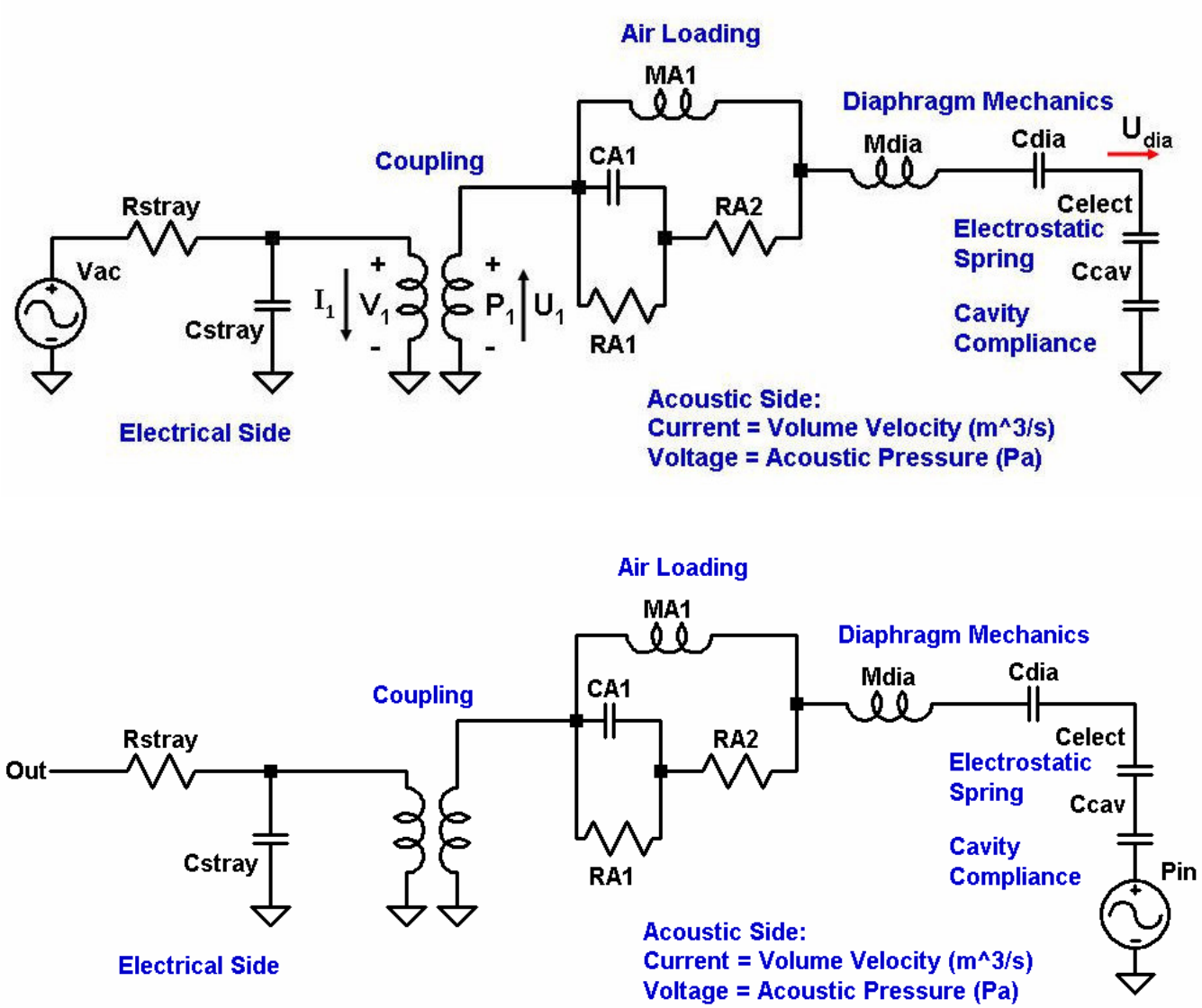

FIGURE 1: MECHANICAL-ELECTRICAL LUMPED ELEMENT MODEL OF THE TRANSDUCER IN TRANSMIT MODE (TOP) AND RECEIVE MODE (BOTTOM).

element's diaphragm. In transmit mode, the output of the model is the diaphragm's volume velocity, U_{dia}, which can be used to compute the farfield transmitted pressure, as discussed later in the paper. The bottom model represents the element while in "receive" mode. In "receive" mode, an external acoustic pressure, P_{in}, is applied to the diaphragm face. The result is a volume velocity which is converted to a current by the ideal transformer, feeding from there into the receive electronics.

The lumped element acoustic model incorporates environmental loading, diaphragm mass, diaphragm acoustic compliance, the negative electrostatic spring, and backing cavity compliance. Many of these elements were calculated analytically using known acoustic parameters [6-7].

The environmental impedance, Z_{env}, was computed using the four components for a rigid baffled piston radiating into an infinite half space for, valid for $(\omega a/c) < 2$ [7],

$$Z_{env} = [M_{A1} s(R_{A1} + R_{A2} + C_{A1} R_{A1} R_{A2} s)] \cdot [C_{A1} M_{A1} R_{A1} + (M_{A1} + C_{A1} R_{A1} R_{A2}) + R_{A1} + R_{A2}]^{-1} \quad (1)$$

$$R_{A1} = 0.1404 \rho c / a^2 \quad (2)$$

$$R_{A2} = \rho c / (\pi a^2) \quad (3)$$

$$M_{A1} = 8\rho / (3\pi^2 a) \quad (4)$$

$$C_{A1} = (5.94 a^3) / (\rho c^2) \quad (5)$$

where ρ and c represent the speed of sound and density for the environment, and s represents the Laplace transformation variable. The diaphragm moves in a bending shape as opposed to a perfect rigid piston. Therefore, a, representing the effective diaphragm radius, is equal to 80% of the physical radius for a bending circular plate, as determined using finite element analysis.

The electrostatic spring, C_{elect}, is the only nonlinear element in the model, but it can be treated as a short circuit as long as the bias voltage on the transducer is not approaching the pull-in voltage. If it cannot be treated as a short circuit, then the negative acoustic compliance associated with the electrostatic spring can be determined,

$$C_{elect} = A / K \tag{6}$$

where A represents the surface area of the diaphragm, and K represents the electrostatic spring (force/distance) of the transducer. In order to calculate K, linearized about a nominal deflection, d_{nom}, the following equation is used,

$$K = -\left(\frac{d_{nom}}{\varepsilon_1} + \frac{d_2}{\varepsilon_2} + \frac{d_3}{\varepsilon_3}\right)^{-3} \cdot \left(\frac{1}{\varepsilon_1^2}\right) \cdot \left(V_{bias}^2\right) \tag{7}$$

In calculating the electrostatic spring equation, d_{nom} is the nominal height of the vacuum gap, ε_1 is the permittivity of free space, d_n and ε_n are the height and permittivity of the other intervening dielectric layers, and V_{bias} is the applied DC bias. It is important to note that K should have a negative value.

For cMUTs with a low vacuum backing cavity, the compliance of the backing cavity may not contribute much stiffness, but may be easily included. Within the transducer model, there is a small vacuum filled cavity located within the transducer, filled with a small amount of residual air. This acts as a small mechanical spring as it is compressed by the motion of the diaphragm. The cavity compliance can be calculated by

$$C_{cav} = V_{cav} / \left(\rho_{cav} c^2\right) \tag{8}$$

where V_{cav} is the volume of the cavity, c is the speed of sound (not strongly affected by pressure), and ρ_{cav} is the density of the rarefied air in the cavity, which may be approximated by

$$\rho_{cav} = \rho_0 \frac{P_{cav}}{P_0} \tag{9}$$

where the density in the cavity is the density of air at atmospheric pressure, ρ_0, multiplied by the ratio of the cavity pressure to atmospheric pressure.

Finite Element Analysis

Due to the complex cross-sectional geometry of the transducer designs, finite element analysis was used to determine the diaphragm stiffness, effective diaphragm mass, and the electrostatic coupling for the transducer.

COMSOL Multiphysics ® was used to map the complex geometry of each transducer as an axisymmetric cross-section. A basic layout of the transducer's cross section can be seen in Figure 2. In each case, the transducer is structured as an axisymmetric cross-section, comprised of a bulk silicon base, several thin film dielectric layers, and a passivation layer. Within the diaphragm region rests a top and bottom conductor, as well as a vacuum-filled cavity resting in between the two. The two conductive layers form the variable parallel plate capacitor for electrical-mechanical coupling. The air gap acts as a small mechanical spring, mentioned in the above section.

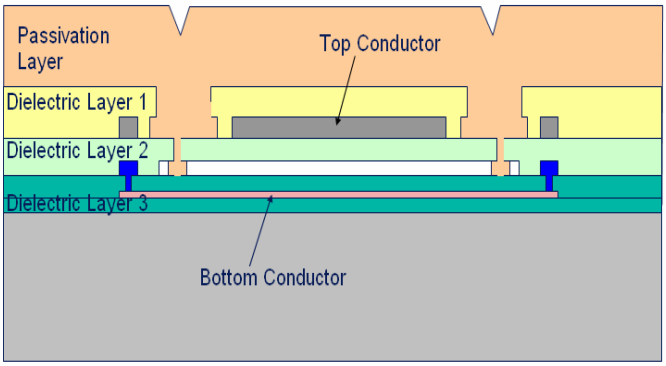

FIGURE 2: AXISYMMETRIC CROSS-SECTION OF THE TRANSDUCER.

C_{dia}, representing the *in vacuo* diaphragm acoustic compliance, was calculated using a linear elastic axisymmetric static analysis. The acoustic compliance is the surface integral of air displaced by the diaphragm at DC in response to a unit applied pressure on the face of the transducer. A lower compliance indicates a stiffer diaphragm. An eigenfrequency analysis was then performed on the same model in order to determine the diaphragm effective mass, M_{dia} according to

$$\frac{1}{\sqrt{M_{dia} \cdot C_{dia}}} = f_1 \cdot 2\pi \tag{10}$$

where f_1 is the first eigenfrequency in cycles per second. The FEA computation was originally conducted for a transducer with a passivation layer comprised of PECVD nitride. However, a number of scenarios utilizing different passivation layer materials, including Oxynitride and Parylene-C, as well as no passivation layer at all, were computed as well.

Coupling can be computed by considering the parallel plate capacitor formed between the aluminum and the doped polysilicon with the two intervening dielectrics and the vacuum gap,

$$N = \alpha\left(\frac{d_{nom}}{\varepsilon_1}+\frac{d_2}{\varepsilon_2}+\frac{d_3}{\varepsilon_3}\right)^{-2}\cdot\left(\frac{1}{\varepsilon_1}\right)\cdot V_{bias} \quad (11)$$

Note that N has units of *Pa/V*, or, equivalently, *Amp/(m/s)* (in SI units). It is a bidirectional coupling constant for the ideal transformer.

Alpha, α, is a nondimensional parameter to account for incomplete electrode coverage, where $0< \alpha<1$. When a transducer is in "receive" mode, it is driven by a uniform pressure applied to the top of it's diaphragm, in which a volume displacement is determined for the entire diaphragm, U_1. However, when in "transmit" mode, the uniform pressure is applied only to the electrodes, and a different volume displacement, U_2, is obtained. α is computed by using FEA to run the two static simulations, and then applying the results to the following equation,

$$\alpha = U_2 / U_1 \quad (12)$$

where different values for α will be obtained based on the geometry and material properties of the transducer.

With these parameters in hand, the volume velocity in response to a given DC bias plus RF drive voltage can be computed. This volume velocity can be translated into a membrane centerpoint displacement by

$$u = \frac{u_{ctr}U_{dia}}{j\omega} \quad (13)$$

where u_{ctr} is the ratio of the centerpoint displacement to the volume displacement taken from the static finite element computation. The pressure at a distance r from the element can also be estimated by treating the element as a baffled simple source, assuming we are in the farfield and there are no reflections,

$$P(r,t) = U_{dia}\frac{\rho f}{r}e^{j\omega\left(t-r/c\right)} \quad (14)$$

where e is the density of the environment, f is the frequency of the drive, and c is the sound speed in the environment.

Based on the above equations, and the acoustic models displayed in Figure 1, the transmit dynamics can be represented by the following transfer function,

$$H_1(s) = \frac{U_{dia}(s)}{V^2(s)} = \frac{N\cdot s}{M_{dia}s^2 + Z_{env}(s)\cdot s + \left(1/C_{dia}+1/C_{cav}+1/C_{elect}\right)} \quad (15)$$

Note that this is the volume velocity of the membrane, U_{dia}, in response to the square of the applied voltage. Thus, if we are interested in the response at ω when driving with a DC bias, V_{dc}, plus an AC pure tone at ω, with amplitude V_{ac}, the volume velocity magnitude will be $|H_1(j\omega)|$ multiplied by $2V_{dc}V_{ac}$.

The receive dynamics can be represented by a second transfer function,

$$H_2(s) = \frac{U_{dia}(s)}{P(s)} = \frac{-s}{M_{dia}s^2 + Z_{env}(s)\cdot s + \left(1/C_{dia}+1/C_{cav}+1/C_{elect}\right)} \quad (16)$$

where P is an external driving pressure. It is important to note that P here does *not* include the pressure generated by the element in question, that loading is accounted for the in the environmental impedance, Z_{env}. However, the external pressure could come from pressures generated by other cMUTs in the array, as will be discussed in a later section of this paper.

The use of these transfer functions results in the creation of the frequency response plots displayed in the next section.

SINGLE ELEMENT RESULTS

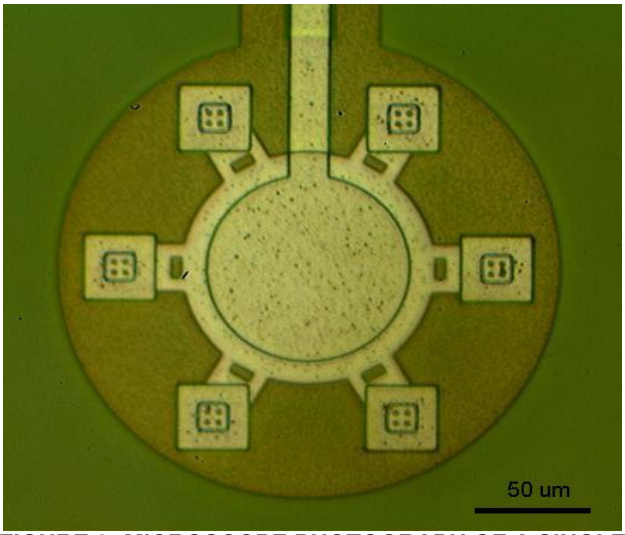

FIGURE 3: MICROSCOPE PHOTOGRAPH OF A SINGLE CMUT ELEMENT.

Using the computational model, frequency response plots were generated for a single element of the array in both air and water environments. The models were also tested with different passivation layer materials and thicknesses. A sample frequency response plot can be seen in Figure 4. In air, the primary resonance for this device is predicted to be 6.1 MHz, with a very narrow fractional bandwidth of 0.2%. In the underwater environment, the model predicts a 3.4 MHz center frequency, with a fractional bandwidth of 27% for the same device. As a comparison, experimental results for transmit operation in a water tank indicate an approximate center frequency for this device of 3.3 MHz with 50% fractional bandwidth.

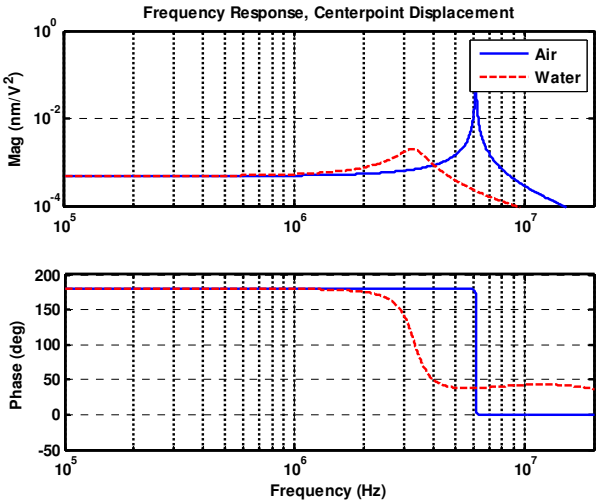

FIGURE 4: MODELED TRANSMIT FREQUENCY RESPONSE FOR A SINGLE ELEMENT IN AIR AND WATER ENVIRONMENTS.

A frequency sweep test was also performed on a single element transducer, in air, with a +9 V_{DC} bias and a 2 V_{PP} RF input. Laser Doppler velocimetry (LDV) was used to measure the membrane centerpoint response. Test results show a peak frequency of about 5 MHz, with an approximate 0.01 nm/V^2 low-frequency gain.

Centerpoint displacement calculated from the computational model was compared to the frequency sweep data obtained from the single cMUT element transducer. The computational model predicted a peak frequency of approximately 6 MHz, similar to the 5 MHz obtained from the transducer chip. The experimental results show considerably larger displacements at low frequencies than the model predicts. A frequency plot comparison can be seen in Figure 5. The magnitude is the amplitude of the centerpoint displacement normalized to the product of the applied DC bias and the amplitude of the RF drive voltage.

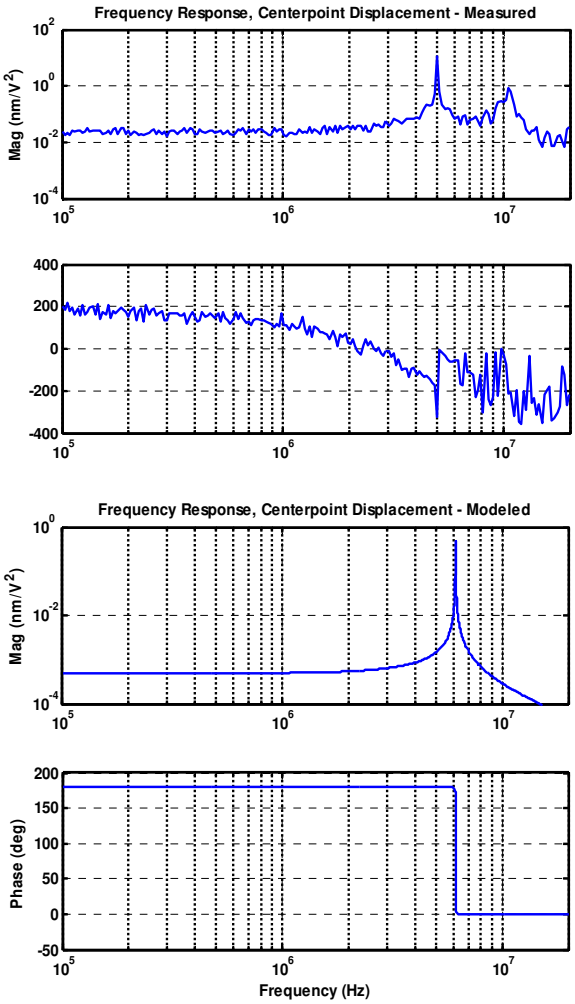

FIGURE 5: FREQUENCY RESPONSE COMPARISON BETWEEN COMPUTATIONAL AND EXPERIMENTAL DATA.

Using LDV, a transient step response was measured for a single element in air, for a 0 to 10 V step. The result is

shown in Figure 6. The step response shows the very high Q of the system when operating in air, and a resonant frequency of 5 MHz, similar to the high-Q 6 MHz resonance predicted by the model. The Q of the system decreases dramatically when submerged, both in computation and in water tank experiments. Model results illustrating this appear in Figure 4.

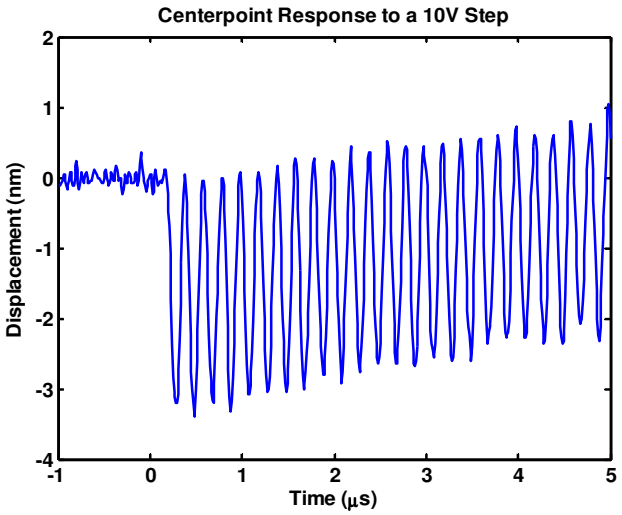

FIGURE 6: A 10 V TRANSIENT STEP RESPONSE OF A SINGLE TRANSDUCER ELEMENT (LDV MEASUREMENT).

ARRAY COMPUTATIONS AND RESULTS

Array computations have been carried out for a 55 element columnar array, an example of which can be seen in Figure 7.

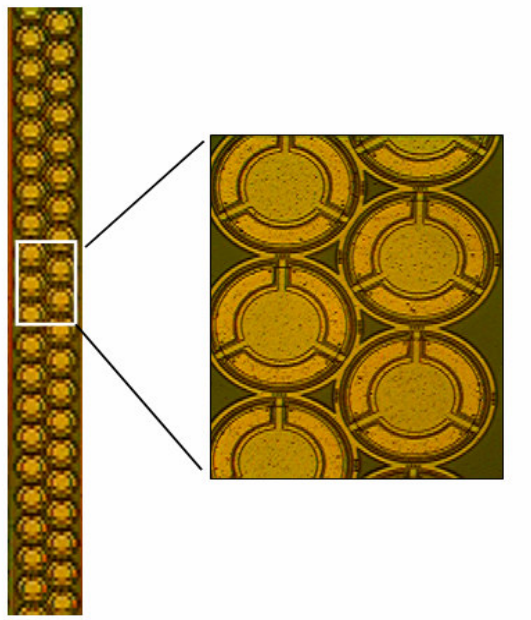

FIGURE 7: MICROSCOPE PHOTOGRAPH OF A 55 ELEMENT COLUMNAR ARRAY.

In the coupled computation, each element is forced not only by the electrostatic force but also by the pressures generated by the motion of all other elements in the array. This leads to a matrix computation, with a fully populated transfer function matrix including the phase lag and geometric spreading of the baffled monopole pressure field for each individual element. The unknowns in the equation are the volume velocities of the elements in the array, which can be calculate using the following equation,

$$U_m = H_1(s)V_m^2 + \sum_{n=1}^{elements}[H_2(s)P_{mn}(1-\delta_{mn})] \qquad (17)$$

where δ_{mn} is the Kronecker delta function, and P_{mn} is the pressure field produced by the n^{th} element at the m^{th} element's centerpoint. This pressure is a direct function of the volume velocity of the n^{th} element,

$$P_{mn} = \frac{\rho}{2\pi}\frac{1}{R_{mn}} s e^{-\frac{R_{mn}}{c}s} U_n \qquad (18)$$

where R_{mn} is the distance between the m^{th} and n^{th} elements, s is the derivative operator, and e^{-Ts} is the delay operator. For steady state, harmonic drive computations, s may be replaced with $j\omega$, resulting in an algebraic matrix inversion to find the complex volume velocities. The transfer functions $H_1(s)$ and $H_2(s)$ were given in equations (15) and (16).

Once the volume velocities for all elements are determined from the coupled computation, the farfield pressure can be computed by summing the monopole fields from each element,

$$P(x,y,z,t) = \frac{\rho}{2\pi}\cdot\sum\frac{1}{R_m}\cdot sU_m\cdot(t-R_m/c) \qquad (19)$$

where the radial distance, R_m, from the m^{th} element to the field point is

$$R_m = \sqrt{(x_m-x)^2+(y_m-y)^2+(z_m-z)^2} \qquad (20)$$

The array computation shows a considerable increase in bandwidth for the array over the bandwidth of an individual element. Figure 8 compares the predicted pressure for the 55 element columnar array transmitting into water at a

distance 7.5 mm from the center of the array for a 40 V_p pure AC drive. The two curves in the plot represent the result when each element in the array transmits in isolation (labeled "uncoupled"), and when the fully coupled solution is computed.

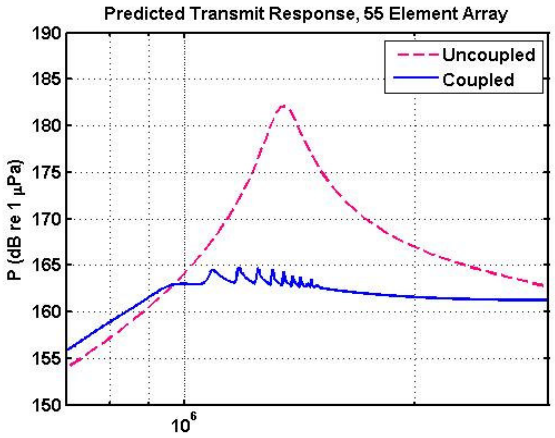

FIGURE 8: COMPARISON BETWEEN COUPLED AND UNCOUPLED COMPUTATIONS.

Frequency sweep tests were performed on several column array elements grouped together on a single transducer. Some of the element arrays tested had been shorted out during wirebonding, but were measured for comparison purposes. Similar to the frequency sweep for the single element transducer, the tests were performed in air, with a +9 V_{DC} bias and a 2 V_{PP} RF input. The obtained results can be seen in Figure 9.

Tests results show a peak frequency of about 2.2 MHz, with an approximate 0.01 nm/V^2 low-frequency gain for the active driven columns. While the shorted column arrays showed a similar 0.01 nm/V^2 low-frequency gain, the results showed that peak frequency occurred much lower, at about 0.3MHz.

Columns adjacent to the ones being driven were also tested. The arrays adjacent to the shorted out columns showed similar results. The arrays adjacent to the active columns did not respond at the peak frequency

CONCLUSIONS

A method of combining FEA and lumped element modeling for cMUT elements has been described. The modeling method is computationally efficient, and leads to good predictions of the resonant frequency and bandwidth of individual elements in both air and water environments. The low frequency magnitude of the computation does not yet agree well with measurements; additional investigations are underway to determine if this is a modeling or measurement artifact. Array computations have been briefly described. The bandwidth predicted by a fully coupled computation is much wider than the uncoupled result

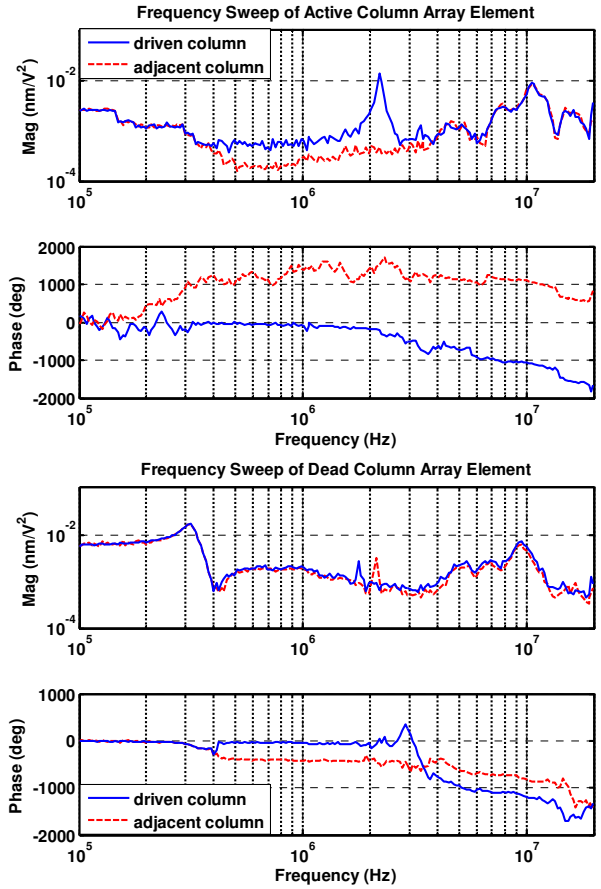

FIGURE 9: FREQUENCY RESPONSE COMPARISON BETWEEN ACTIVE AND DEAD COLUMN ARRAY ELEMENTS.

REFERENCES

1. Ladabaum, I., Jin, X., Soh, H., Atalar, A., and Khuri-Yakub, B. *Surface Micromachined Capacitive Ultrasonic Transducers.* IEEE Transactions on Ultrasonics, Ferroelectrics, and Frequency Control, 1998, **45**(3): p. 678-690.

2. Jin, X., Ladabaum, I., Degertekin, F., Calmes, S., and Khuri-Yakub, B. *Fabrication and Characterization of Surface Micromachined Capacitive Ultrasonic Immersion Transducers*. IEEE Journal of Microelectromechanical Systems, 1999, **8**(1): p. 100-114.

3. Lohfink, A., Eccardt, P.-C., Benecke, W., and Meixner, H. *Derivation of a 1D CMUT Model from FEM Results for Linear and Nonlinear Equivalent Circuit Simulation*. IEEE Ultrasonics Symposium, 2003: p. 465-468.

4. Yaralioglu, G., Badi, M., Ergun, A., and Khuri-Yakub, B. *Improved Equivalent Circuit and Finite Element Method Modeling of Capacitive Micromachined*

Ultrasonic Transducers. IEEE Ultrasonics Symposium, 2003: p. 469-472.

5. Hansen, S., Turo, A., Degertekin, F., and Khuri-Yakub, B. *Characterization of Capacitive Micromachined Ultrasonic Transducers in Air Using Optical Measurements*. IEEE Ultrasonics Symposium, 2000: p. 947-950.

6. Kinsler, L., Frey, A., Coppens, A., and Sanders, J. *Fundamentals of Acoustics: Fourth Edition*. John Wiley & Sons, Inc. 2000.

7. Beranek, Leo. *Acoustics*. American Institute of Physics. 1986.